J. Fluid Mech. (1996), *vol.* 311, *pp.* 193–217

Forced unidirectional infiltration of deformable porous media

By JARED L. SOMMER† AND ANDREAS MORTENSEN
Department of Materials Science and Engineering, Massachusetts Institute of Technology, Cambridge, MA 02139, USA

(Received 7 April 1994 and in revised form 25 July 1995)

We treat the infiltration of an initially dry deformable porous medium by a pressurized liquid, taking into account the influence of variations in permeability within the deformed porous medium. Chief assumptions of our analysis are neglect of gravity, of inertial forces, and of partial saturation in the porous medium. We focus on unidirectional infiltration under constant liquid pressure, and present data from the infiltration of polyurethane sponge by ethylene glycol in a configuration of nearly unidirectional infiltration with reflief from friction effects along sample sides. We find excellent agreement between theory and experiment at longer infiltration times. We examine an additional assumption, namely the neglect of solid-phase velocity compared with average local liquid velicity at lower porous-medium strains. Agreement of this simplified model with experimental data, albeit less good, remains quite acceptable given the considerable computational simplicity it produces.

1. Introduction

One of the principal composite material production techniques is infiltration, by which a matrix material in liquid form is injected into a porous solid perform of reinforcing phase elements such as fibres, whiskers or particles. In this process, the liquid matrix is often pressurized to speed the rate of production of the composite, and to overcome capillary forces which may oppose entry of the fluid into the preform. Applied pressure, and the frequently high compliance of the porous preforms, can cause significant preform deformation during infiltration (e.g. Gutowski, Morigaki & Cai 1987; Yamauchi & Nishida 1995). This deformation, in turn, influences the rate of flow of the liquid into the preform, and the microstructure of the resulting material.

The flow of liquids through deformable media is a class of problems that has relevance in various other contexts, including biomechanics, magma mechanics, ground water hydrology, soil consolidation and reservoir engineering. Governing mechanics of this process are well understood; however coupling between flow of the fluid and mechanical deformation of the solid causes the formulation and solution of this class of problems to be sufficiently involved that simplifying assumptions are often invoked.

This paper examines assumptions appropriate when pressure driving liquid into a dry porous medium is high in comparison with the range of capillary pressures characteristic of wetting of the porous medium by the liquid. The simplifications we use are based on the observation that permeability K of a porous medium depends strongly on the pore volume fraction θ within this medium: using the Kozeny–Carman expression K is proportional to $\theta^3(1-\theta)^{-2}$ (Philip 1968). For $\Delta\theta = 0.1$, then, K always

† Present address: Technical Research Associates, Salt Lake City, UT, USA.

changes by more than 100%, and by substantially more for θ near one or zero. In pressurized infiltration, therefore, the permeability cannot be taken to be constant if deformation of the porous medium is significant, contrary to what is often assumed in 'small-strain' flow through deforming porous media (e.g. Bear 1972; Scheidegger 1974; Bear & Bachmat 1990).

'Small-strain' assumptions were relaxed by Philip and co-workers for several basic problems of fluid flow through deformable porous media, with a focus on flow of water through swelling clay-based soils. These authors extended the Boltzmann transformation commonly used to treat the unidirectional infiltration of non-deforming media to the analysis of unidirectional gravity-free infiltration into swelling media, using Eulerian as well as Lagrangian coordinates (Philip 1968, 1969*a*, *b*). These features of the work by Philip and co-workers are incorporated in the analysis presented here. Experimental confirmation of the predicted time-dependence resulting from validity of the Boltzmann transformation has been reported for unidirectional infiltration into swelling soils (Smiles & Rosenthal 1968; Smiles & Colombera 1975; Angulo *et al.* 1990*a*, *b*).

Because prediction of the rate of infiltration with pressurized liquid is so strongly dependent on prediction of local variations in K within the infiltrated porous medium, other features of the problem can often be neglected. In particular, the gradual progress of wetting, of importance in soils because pressures driving the liquid are of the same order as capillary pressures, can often be ignored and replaced with the assumption that complete saturation takes place at a single pressure, along a well-defined two-dimensional infiltration front. This simplifies considerably the problem compared with the case where liquid and gas coexist over finite distances, because the permeability of the medium and the volume-fraction liquid become single functions of strain. A further approximation we propose is to ignore the solid-phase velocity in Darcy's law when porous medium strains are sufficiently large to cause significant variations in permeability, yet not so large as to cause the solid to move faster than the liquid. This additional approximation yields somewhat less precise predictions, but simplifies mathematical solution of the problem very significantly.

We begin this article by describing our assumptions and analysing the problem of one-dimensional pressure infiltration of an initially dry and highly deformable porous medium. We focus on the case of a constant applied pressure driving the fluid into the porous medium, and use in our analysis the Boltzmann transformation in Eulerian coordinates first proposed by Philip (1968). We then present experimental data from a simulation of one-dimensional frictionless infiltration, and show that for the porous solid material strains of our experiment (the porous material density varies by about 100%), the analysis compares well with experiment.

2. Theory

2.1. *General problem statement and assumptions*

We consider the infiltration of a porous medium by liquid injected under constant applied pressure over a portion of the outer surface of the porous medium. We assume that the liquid and the solid porous medium are at the same temperature everywhere and at all times.

We simplify all capillarity effects by assuming that infiltration takes place at a single capillaric pressure. Infiltration is therefore taken to occur along a well-defined two-dimensional infiltration front, across which the porous medium goes from completely dry to fully saturated (this is often called the *slug-flow* assumption). This assumption,

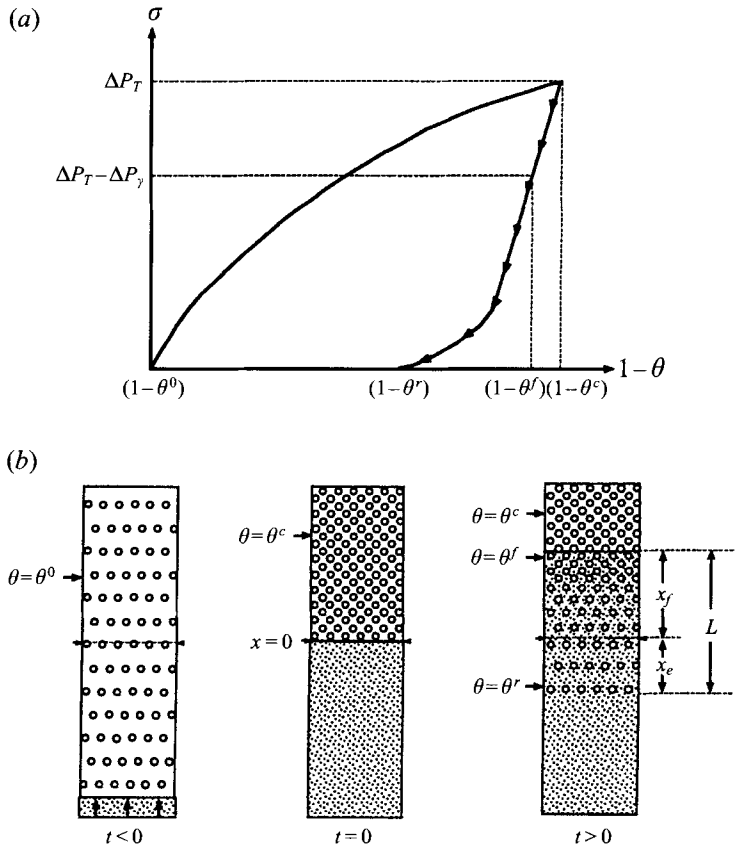

FIGURE 1. (*a*) Schematic illustration showing the uniaxial compression behaviour of a dry porous solid during infiltration by a non-wetting liquid under a constant applied pressure ΔP_T. (*b*) The same solid before and during infiltration by a non-wetting liquid under a constant applied pressure ΔP_T.

made previously in the context of soil infiltration experiments (Green & Ampt 1911), is poorly justified in some cases (for example in the low-pressure infiltration of swelling soils treated by Philip & Smiles (1969); however there are many other instances, including composite material infiltration processing, in which this assumption has been shown to be legitimate for non-deforming porous media (Bear 1972; Dave 1990; Yang, Zografi & Miller 1988; Masur *et al.* 1989; Mortensen *et al.* 1989; Mortensen & Wong 1990). In particular, this assumption is legitimate when the applied pressure exceeds significantly the capillary pressure change ΔP_γ accompanying full infiltration of pores within the preform; in composite material processing, this is often the case. We note that the sign of ΔP_γ varies depending on wetting characteristics of the porous medium: ΔP_γ is negative when the liquid 'wets' the preform material, into which it is spontaneously drawn. When $\Delta P_\gamma > 0$, flow of the liquid is resisted by capillary forces and pressure must be applied to drive the liquid into the dry porous medium.

We assume that gas ahead of the front is easily expelled through the uninfiltrated portion of the porous preform, offering negligible resistance to flow because of its comparatively low viscosity. The pressure within the gas that occupies the uninfiltrated portion of the preform is then constant. We assume that the liquid and solid materials themselves are incompressible, but let the porous solid medium deform macroscopially under applied external stress. We assume that infiltrated pores are very small in

comparison to the dimensional scale of the porous medium. The volume fraction of open pores in the dry porous material, or of liquid in the infiltrated portion of the porous material, is defined as θ. The local volume fraction of solid and closed porosity is therefore $(1-\theta)$ everywhere.

We neglect body forces, including gravitational forces. This assumption is valid when pressure gradients within the infiltrated portion of the porous medium, estimated as the applied pressure divided by the infiltration depth, are larger than the sum of all body forces in the fluid. We also neglect inertial forces, both within the preform and within the flowing liquid, by comparison with viscous forces at the boundary between the liquid and solid phases. At the infiltration front, we therefore take the change in local preform strain due to passage of the sharp infiltration front, and its concommittant pressure drop ΔP_γ, to be instantaneous. At the microscopic level, we therefore also assume that the porous-medium flow Reynolds number $Re \leqslant 1$ (see §5.1(i)), so that fluid flow follows Darcy's Law. If the average local velocity of the liquid within the pores is $\boldsymbol{u}_l$, and $\boldsymbol{u}_s$ is the average local velocity of the solid measured in the same reference frame as $\boldsymbol{u}_l$, we then have

$$\boldsymbol{u}_l - \boldsymbol{u}_s = -\frac{\boldsymbol{K}}{\theta\mu} \cdot \nabla P, \tag{1}$$

where $\boldsymbol{K}$ is the permeability tensor of the porous medium, μ the liquid viscosity, and P the pressure in the liquid (Biot 1955; Philip 1968).

Mass conservation in the solid and liquid phases, respectively, yields

$$\frac{\partial\theta}{\partial t} - [\nabla \cdot (1-\theta)\,\boldsymbol{u}_s] = 0 \tag{2}$$

and

$$\frac{\partial\theta}{\partial t} + [\nabla \cdot \theta \boldsymbol{u}_l] = 0. \tag{3}$$

Having neglected inertial and body forces in both solid and liquid, stress equilibrium dictates:

$$\frac{\partial P}{\partial x_i} + \sum_{j=1}^{3} \frac{\partial \sigma_{ij}}{\partial x_j} = 0, \tag{4}$$

where x_i are coordinate axes, and σ_{ij} are components of the effective stress tensor acting in the solid along these axes, counted as positive in compression and averaged over a surface area comprising both solid and liquid. The effective stress, which equals the actual average stress in all material within ΔV minus the fluid pressure P, determines the macroscopic deformation of the fully saturated porous material in ΔV (Nur & Byerlee 1971).

We make no particular assumptions concerning the response to stress of the porous solid material. In particular, the relation between stress and strain may be irreversible: in composite fabrication this is often the case because deformation of the perform often breaks, deforms, or displaces individual solid elements (such as fibres) that constitute the porous material.

2.2. *Unidirectional infiltration under constant applied pressure*

We focus on the case of unidirectional infiltration, in which both flow and strain take place only along the x-direction, and we assume that the applied pressure is constant. We assume that the porous medium is initially homogeneous, isotropic in a plane

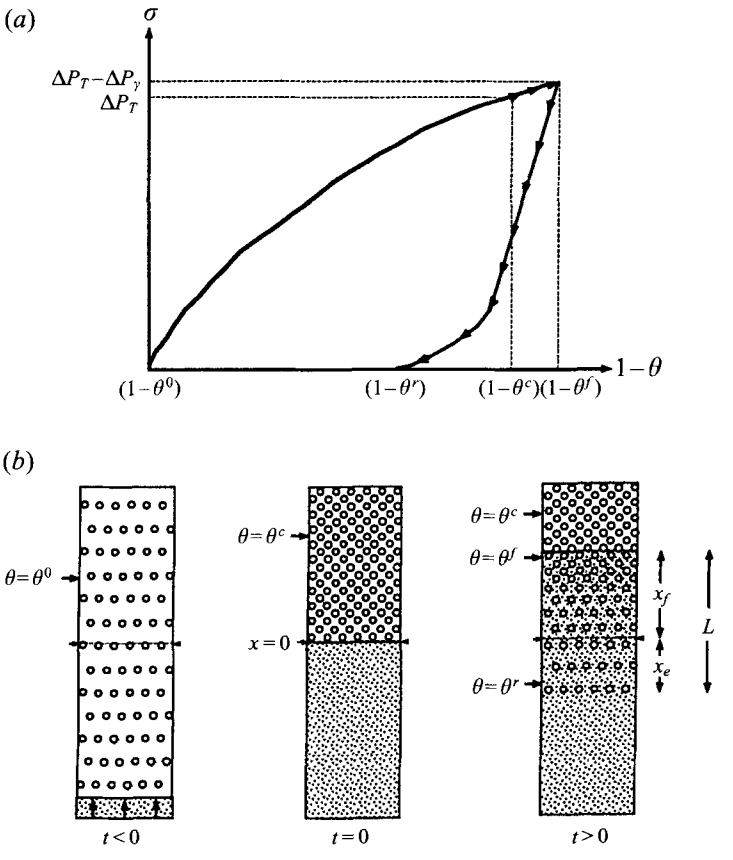

FIGURE 2. As figure 1 but during infiltration by a wetting liquid under a constant applied pressure ΔP_T.

perpendicular to the x-axis (such that the infiltration direction is a principal direction of the preform permeability tensor) and that its response to stress is independent of time and rate. The liquid penetrates the porous material at one end, infiltrating it toward the other, fixed, end under a constant applied pressure P_0, applied on the liquid at the entrance of the porous medium. The constant pressure difference driving the flow is thus $\Delta P_T = P_0 - P_g$, where P_g is the gas pressure in the uninfiltrated porous material.

The stress–strain curve measured on the porous medium by unidirectional compression tests with zero lateral strain is schematically depicted in figures 1(*a*) and 2(*a*), for loading to ΔP_T and unloading to zero stress. This curve can be measured on a dry sample of the porous material if its mechanical response is unaffected by contact with the fluid. During infiltration, in the very first moments of contant between the liquid and the preform, there is a transient period during which the liquid is decelerated by the porous medium, which simultaneously is rapidly compressed to a volume fraction $(1-\theta) = (1-\theta^c)$, corresponding to $\sigma_{xx} = \Delta P_T$ on the stress–volume-fraction curve. As mentioned above, we do not consider the dynamics of this short initial transient, during which inertial effects play a dominant role, at the macroscopic level (since solid and liquid experience substantial accelerations), and also at the microscopic level (since $Re > 1$). We focus on subsequent moments of the process, and to this end simplify the problem by taking compression of the porous material to be instantaneous and Darcy's law to be valid throughout infiltration.

At time $t = 0$, the infiltration front is then at the entrance of the porous material, which is compressed under the full applied pressure ΔP_T, figures 1(*b*) and 2(*b*). Later, at $t > 0$, as the infiltration front passes, it engulfs a slice dx of the porous material, which sees its effective stress suddenly altered by the capillary pressure ΔP_γ.

If $\Delta P_\gamma > 0$, i.e. if the liquid does not wet the porous material, the porous material immediately behind the front therefore relaxes somewhat, following the unloading stress–strain curve. Its strain therefore decreases, to a value given by the unloading portion of the stress–strain curve at $\sigma_{xx} = \Delta P_T - \Delta P_\gamma$. Conversely, if $\Delta P_\gamma < 0$, corresponding to wetting by the liquid, the porous medium contracts somewhat, first climbing further up the loading stress–strain curve to $\sigma_{xx} = \Delta P_T - \Delta P_\gamma$. This capillarity-driven change in preform strain is negligible if ΔP_γ is small, but can be significant in some systems (in infiltration by a molten metal, the high surface energies involved can cause ΔP_γ to be on the order of 1 MPa (Mortensen & Wong 1990)). We note that by neglecting irreversible losses in the wetting process, ΔP_γ can be estimated as (Mortensen 1990)

$$\Delta P_\gamma = -S_f \sigma_{LA} \cos(\alpha), \tag{5}$$

where α is the contact angle of the liquid metal on the flat solid substrate material, σ_{LA} is the liquid matrix surface energy, and S_f is the total surface area of the solid phase per unit volume of pores immediately ahead of the infiltration front.

From behind the infiltration front to the preform entrance, the liquid pressure P increases from $\Delta P_\gamma + P_g$ to P_0, and the effective stress σ_{xx} acting on the porous medium correspondingly decreases to zero. The compressive strain on the porous medium therefore decreases toward the entrance, following the stress–strain curve for unloading from $\Delta P_T - \Delta P_\gamma$. Since θ increases with distance from the infiltration front, the pressure gradient within the infiltrated portion of the porous material decreases with distance from the infiltration front because the permeability K increases rapidly with increasing θ. Two general features of the process are, therefore, that most relaxation of the porous material takes place near the infiltration front, and that this region constitutes a narrow 'bottleneck' to flow of the liquid.

The infiltration kinetics and the shape of the porous material during infiltration are related, and must be solved together. We use Eulerian (fixed) coordinates, and define the position to which the preform entrance is initially compressed as $x = 0$. The x-axis is therefore fixed in relation to the uninfiltrated end of the preform. In what follows, we drop the suffix x from vectorial or tensorial components. Governing equations (1)–(4) then become

Darcy's Law:
$$u_l - u_s = \frac{-K}{\theta\mu}\frac{\partial P}{\partial x}, \tag{6}$$

solid conservation:
$$\frac{\partial \theta}{\partial t} - \frac{\partial((1-\theta)u_s)}{\partial x} = 0, \tag{7}$$

liquid conservation:
$$\frac{\partial \theta}{\partial t} + \frac{\partial(\theta u_l)}{\partial x} = 0, \tag{8}$$

stress equilibrium:
$$\frac{\partial P}{\partial x} = -\frac{\partial \sigma}{\partial x}. \tag{9}$$

We use the Boltzmann transformation to convert these partial differential equations into ordinary differential equations involving dimensionless parameters compatible

with the initial and boundary conditions of the problem at hand. To this effect, we define χ as

$$\chi = \frac{x - x_e}{\psi t^{1/2}}, \tag{10}$$

where x_e is the position of the porous preform entrance at time t, and Ψ is a constant. In our experiment, and in figures 1 and 2, the preform relaxes; hence $x_e < 0$. ψ is chosen such that the position of the infiltration front corresponds to $\chi = 1$:

$$L = \psi t^{1/2}, \tag{11}$$

where L is the total length of the infiltrated portion of the preform, as shown in figures 1 and 2. Taking the partial derivatives of χ with respect to x and t gives

$$\frac{\partial \chi}{\partial x} = \frac{1}{\psi t^{1/2}}, \tag{12}$$

$$\frac{\partial \chi}{\partial t} = -\frac{x - x_e}{2\psi t^{3/2}} - \frac{u_s(\chi = 0)}{\psi t^{1/2}} = -\frac{\chi}{2t} - \frac{u_s(\chi = 0)}{\psi t^{1/2}}. \tag{13}$$

Expansion of Darcy's law and insertion of the stress equilibrium equation (9) yields

$$u_l - u_s = \frac{K}{\theta \mu} \theta' \frac{1}{\psi t^{1/2}} \frac{\partial \sigma}{\partial \theta}, \tag{14}$$

where a prime denotes differentiation with respect to χ. We define dimensionless liquid and solid velocities, l and s:

$$u_l = \frac{\psi l(\chi)}{2t^{1/2}}, \tag{15}$$

$$u_s = \frac{\psi s(\chi)}{2t^{1/2}}; \tag{16}$$

l and s are functions of χ only. Equation (14) now becomes

$$\theta'(\chi) = \frac{\theta \mu \psi^2}{2D(\theta)}(l - s), \tag{17}$$

where, following Philip, we have defined the diffusivity D as

$$D(\theta) = K(\theta) \frac{\partial \sigma}{\partial \theta}.$$

Mass conservation equations (7) and (8) become

$$s' = \frac{\theta'}{(1 - \theta)}(s - s(0) - \chi), \tag{18}$$

and

$$l' = -\frac{\theta'}{\theta}(l - s(0) - \chi), \tag{19}$$

where l' and s' are χ-derivatives of l and s, respectively.

As discussed earlier, each end of the infiltrated portion of the porous medium has its volume-fraction solid fixed by the unloading stress–strain curve for initial compression to ΔP_T. Two boundary conditions follow:

$$\theta = \theta^f \quad \text{at} \quad \chi = 1^-, \tag{20}$$

$$\theta = \theta^r \quad \text{at} \quad \chi = 0, \tag{21}$$

where θ^f is the pore volume fraction at pressure $\Delta P_T - \Delta P_\gamma$, measured from the unloading curve after loading to ΔP_T for a non-wetting liquid, and on the stress–strain curve for further loading to $\Delta P_T - \Delta P_\gamma$ for a wetting liquid. θ^r corresponds to the fully relaxed state of the porous medium after compression to ΔP_T for a non-wetting liquid, and to $\Delta P_T - \Delta P_\gamma$ for a wetting liquid.

Consider a slice of infinitely small thickness $\mathrm{d}x_f$ of the dry porous material immediately ahead of the infiltration front at time t. At t, this slice of porous material is compressed to $\theta = \theta^c$, the volume-fraction porosity in the porous medium compressed under $\sigma = \Delta P_T$ (figures 1*b* and 2*b*). As the infiltration front engulfs an infinitesimal thickness $\mathrm{d}x_f$ of the compressed porous medium, θ changes from θ^c to θ^f, and the width of the porous material changes from $\mathrm{d}x_f$ to $\mathrm{d}x_f + \mathrm{d}x_x$. As the porous medium expands or shrinks, its solid phase thus acquires a finite velocity $u_s(\chi = 1^-)$. A mass balance on the solid at the infiltration front thus dictates that

$$\mathrm{d}x_f(1-\theta^c) = (\mathrm{d}x_f + \mathrm{d}x_x)(1-\theta^f). \tag{22}$$

Therefore

$$u_s(\chi = 1^-) = -\frac{\mathrm{d}x_x}{\mathrm{d}t} = -\frac{\mathrm{d}x_f}{\mathrm{d}t}\frac{\theta^f - \theta^c}{(1-\theta^f)}. \tag{23}$$

The volume of liquid flowing past $x = x_f(t)$ during time interval $\mathrm{d}t$ is $\theta^f u_l(\chi = 1^-)\mathrm{d}t$. This volume of liquid fills pore space $\theta^f \mathrm{d}x_f$ immediately behind the infiltration front; hence

$$u_l(\chi = 1^-) = \frac{\mathrm{d}x_f}{\mathrm{d}t}. \tag{24}$$

Knowing that $x_f = L + x_e$, inserting (15) and (16) into (23) and (24) yields

$$s(\chi = 1^-) = (1 + s(0))\frac{\theta^f - \theta^c}{1-\theta^f}, \tag{25}$$

$$l(\chi = 1^-) = 1 + s(0). \tag{26}$$

Equations (20), (21), (25) and (26) are boundary conditions that must be met in solving (17)–(19) for the parameter ψ and the dimensionless functions $\theta(\chi)$, $l(\chi)$, and $s(\chi)$. We note that in time, a point located at fractional length χ has a constant state (of θ, solid and liquid velocities, etc), and moves proportionally to the square-root of time according to

$$x_\chi = \chi L + x_e = [\chi + s(0)]\,\Psi t^{1/2}, \tag{27}$$

since the preform entrance position x_e is

$$x_e = s(0)\,\Psi t^{1/2}. \tag{28}$$

In particular, the infiltration front is located at

$$x_f = [1 + s(0)]\,\Psi t^{1/2}. \tag{29}$$

A simpler limiting case is obtained if there is no capillary pressure drop across the infiltration front, i.e. if $\Delta P_\gamma = 0$. Then, $\theta^c = \theta^f$ and (25) simplifies to

$$s(\chi = 1^-) = 0. \tag{30}$$

2.3. *Nearly unidirectional infiltration under hydrostatic pressure*

As will be explained in more detail in §3.2, to avoid friction effects along the edge of the deforming porous-medium sample, the experiment we report is one for which the porous medium was strained equally in all three directions while the direction of fluid flow was essentially unidirectional. For comparison of theory with experiment, therefore, we modify slightly the unidirectional infiltration case of §2.2, by replacing the assumption that there is no lateral strain of the porous medium with the assumption that the sides of the porous medium are subjected to a constant hydrostatic pressure equal to P_0. In this configuration, the lateral strain experienced by the porous medium is associated with finite solid velocities in the y- and z-directions as well.

In general, this type of test requires two-dimensional analysis; however when the infiltrated length L is significantly larger than the porous-medium width, and the solid velocity is significantly smaller than the liquid velocity, this configuration requires only a single modification of the mass balance equations, providing a test of the theory free of friction effects.

Having made these assumptions, flow is predominantly in the x-direction and planes initially perpendicular to that direction do not bend appreciably; hence we have

$$\frac{\partial \theta}{\partial y} = \frac{\partial \theta}{\partial z} \approx 0. \tag{31}$$

In the present configuration, effective stress components σ_{xx}, σ_{yy}, and σ_{zz} are equal. If we assume that the porous medium is isotropic, we therefore have $e_{xx} = e_{yy} = e_{zz}$, where e_{ii} is strain in the i-direction. Therefore, $\partial u_{sx}/\partial x = \partial u_{sy}/\partial y = \partial u_{sz}/\partial z$, and substitution of (31) in (2) gives

$$\frac{\partial \theta}{\partial t} - 3(1-\theta)\frac{\partial u_{sx}}{\partial x} + u_{sx}\frac{\partial \theta}{\partial x} = 0. \tag{32}$$

Similarly, insertion of (31) into (3) yields

$$\frac{\partial \theta}{\partial t} + u_{lx}\frac{\partial \theta}{\partial x} + \theta\left(\frac{\partial u_{lx}}{\partial x} + \frac{\partial u_{ly}}{\partial y} + \frac{\partial u_{lz}}{\partial z}\right) = 0. \tag{33}$$

Because lateral velocities are zero along the axis of the porous material, and because there is no relative motion of liquid in relation to the solid along it edges, $\partial u_{ly}/\partial y$ and $\partial u_{lz}/\partial z$ are of the same order of magnitude as $\partial u_{sy}/\partial y$ and $\partial u_{sz}/\partial z$, and hence as $\partial u_{sx}/\partial x$. Since we have assumed that u_{sx} is significantly smaller than u_{lx}, we can neglect $\partial u_{ly}/\partial y$ and $\partial u_{lz}/\partial z$ compared to $\partial u_{lx}/\partial x$. Equation (33) then becomes identical to (8).

Since (32) replaces (7), equation (18) becomes

$$s' = \frac{\theta'}{3(1-\theta)}(s - s(0) - \chi). \tag{34}$$

Except for the factor 3 in the denominator of (18), governing equations of this case are similar to those which govern strictly unidirectional infiltration.

2.4. *Numerical solution of equations*

Nonlinear first-order equations (17), (18) or (34) and (19) were solved numerically, by successive integration of the functions θ, l, and s simultaneously across χ, assuming the initial values for ψ^2, $l(\chi = 0)$, and $s(\chi = 0)$. The mid-point Runge–Kutta scheme was used for integration (Press *et al.* 1989). After integration from $\chi = 0$ to $\chi = 1$, the final values and functions involving θ, l, and s were compared with the boundary conditions (20), (25) and (26). A multi-dimensional Newton–Raphson method was used to adjust the initial guesses of ψ^2, $l(\chi = 0)$, and $s(\chi = 0)$ for convergence. To check for internal consistency within the program, the actual viscous pressure drop was compared with the summation of the drops in pressure over various increments of $\Delta\chi$. The computer program is listed in Sommer (1992).

2.5. *A simple limiting case*

Consider now the case where the average velocity of the solid porous medium is everywhere significantly smaller than the average liquid velocity, $u_s \ll u_l$. By subtraction of (7) and (8) and substitution of (9) into (6), we then have

$$u_l = \frac{K}{\theta\mu}\frac{\partial\sigma}{\partial x} \tag{35}$$

and

$$\frac{\partial(\theta u_l)}{\partial x} = 0. \tag{36}$$

Using the same variable transformation as in §2.2, these become

$$\theta' = \frac{\theta\mu\psi^2 l}{2D} \tag{37}$$

and

$$(l\theta)' = 0. \tag{38}$$

Equation (38) implies, then, that

$$\theta l = \theta^f l(1). \tag{39}$$

Since $u_s \ll u_l$ implies that $|s(0)| \ll 1, l(1) \approx 1$, then

$$\theta l = \theta^f. \tag{40}$$

Insertion of (40) into Darcy's law, (37), then yields

$$-2D\theta'(\chi) = \theta^f\mu\psi^2. \tag{41}$$

By integration of (41), then

$$\int_{\theta}^{\theta^f} 2D(\theta)\,\mathrm{d}\theta = -\theta^f\mu\Psi^2(1-\chi). \tag{42}$$

The constant Ψ, which measures the infiltration rate, can now be simply deduced by setting $\theta = \theta^r$ at $\chi = 0$. The volume-fraction liquid θ and the effective stress σ can then be calculated directly as functions of χ via (42).

Clearly, this solution cannot be rigorous insofar as simple mass conservation dictates that $s(0)$ must differ from zero if there is any relaxation of the porous medium. It can nonetheless provide, even in instances where there is significant relaxation of the preform during infiltration, a reasonable estimation of infiltration kinetics because most resistance to flow of the fluid into the porous medium takes place where the latter

is most compressed (since K decreases strongly as θ decreases), i.e. near the infiltration front, which is precisely where s and v_s are lowest. This solution may therefore provide a valid approximate prediction of infiltration kinetics in many cases since it describes best the 'bottleneck' region of the deformed porous medium. We also note that if it is assumed that Ψ and $\theta(\chi)$ are reasonably approximated by this method of solution, s can be estimated by using (18).

Extension of this approximation to the case treated in §2.3 requires no alteration since we have neglected the displacement of the solid in all equations, with the corollary that the effect of lateral straining of the porous medium is neglected as well.

3. Experimental procedures

3.1. *Material systems*

Type TF-5070-10 polyurethane sponge with a nominal bulk density of 0.159 g cm^{-3}, corresponding to 13.4 volume percent polyurethane (the density of polyurethane is 1.19 g cm^{-3}), was obtained from General Plastics Manufacturing Company, Tacoma, WA. This open-celled polyurethane foam is anisotropic, in that the cells are slightly elongated along one direction, termed the 'rise' direction. Figures 3(*a*) and 3(*b*) are electron micrographs of the sponge used in the experiment, respectively taken parallel and perpendicular to the rise direction.

Prior to testing, the sponges were milled down to 17.8 cm × 4.8 cm × 4.8 cm rectangular parallelepipeds. After machining, the sponge weight and dimensions were measured, to confirm their nominal bulk density value of $\rho_s = 0.159$ g cm^{-3}.

Preliminary experiments on new sponges indicated that their rheological behaviour varies initially with the number of times the sponges are compressed (similar results were found by Parker, Mehta & Caro 1987; Lanir, Sauob & Maretsky 1990; and Beavers, Wittenberg & Sparrow 1981*b*). In order to eliminate this effect, the sponge material was hydrostatically compressed at least 700 times before any experiments, to cause its mechanical behaviour to reach steady state. This was done by enclosing the milled sponge inside a long hermetically sealed plastic bag, and repeatedly evacuating the air out completely and letting air from the open atmosphere back into the sponge. A thin buffer sponge was placed between the bottom of the experimental sponge sample and the vacuum port to ensure that the sponge was pressed uniformly along its length and to ensure uniformity of air flow throughout the sponge during cycling.

To measure volume fractions of the sponge and liquid velocity during infiltration, lines 6.35 mm (0.25 in.) apart were drawn across the width of the sponge, perpendicular to the infiltration direction.

3.2. *Sponge infiltration experiments*

A common experimental difficulty in the experimental investigation of unidirectional flow through deformable porous media arises along the interface between the porous medium and its container, where two conditions must be simultaneously met: (i) the sample must slide free of friction along the inner surface of the container, while (ii) fluid flow between the container and the porous medium must be negligible. These two conditions are difficult to meet simultaneously, because a tight fit of the porous material along the sides of the container tends to produce high friction, while even a small gap causes significant leakage of fluid along the sides of the porous medium (e.g. Lal, Bridge & Collis-George 1970; Beavers, Hajii & Sparrow 1981*a*; Beavers *et al.* 1981*b*). One technique that has been used to circumvent this difficulty is to surround

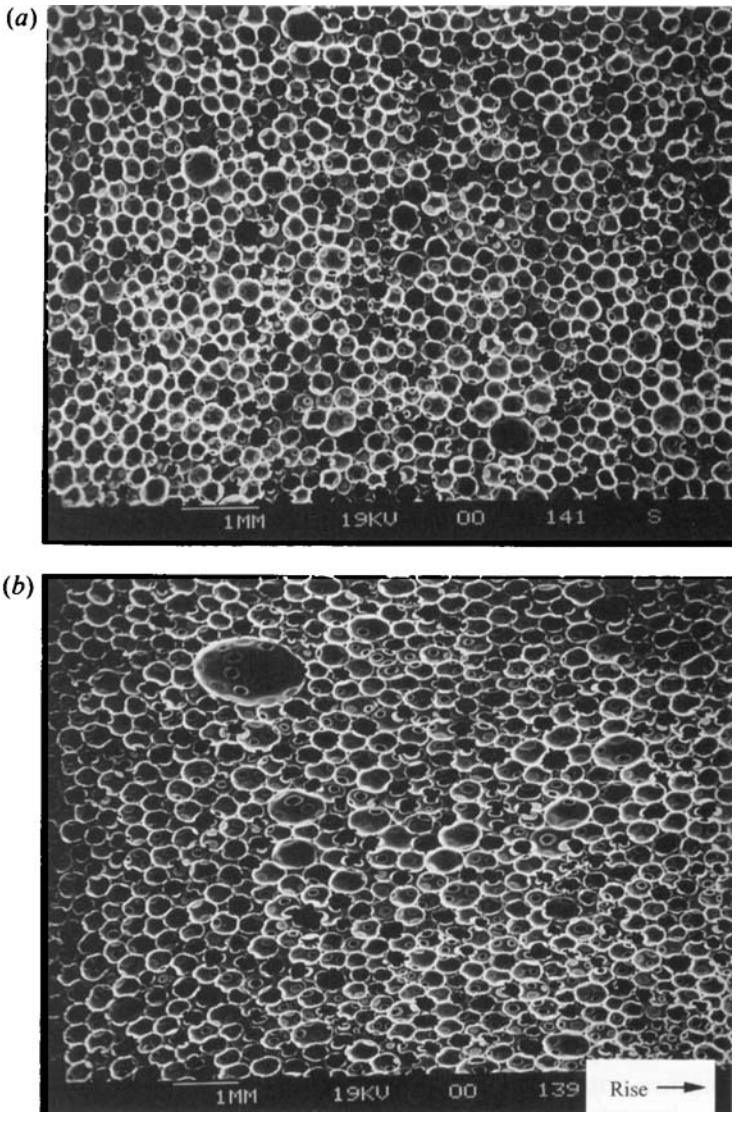

FIGURE 3. Micrograph of the polyurethane foam viewed (*a*) along the rise direction, and (*b*) perpendicular to the rise direction.

the porous medium with several rings, each of which encloses the porous solid tightly, yet slides independently along the container walls (e.g. Smiles & Colombera 1975). This technique has been used with success on soil samples; however friction between the rings and the porous medium still perturbs locally deformation of the solid, and the gap between rings can perturb fluid flow at the outer periphery of the porous medium.

We therefore used an alternative approach, which eliminates these effects. Instead of seeking to prevent flow at the same time as lateral straining along the porous-medium periphery, we embedded a column of porous material in the fluid, leaving its sides free to expand or contract laterally. The liquid was prevented from infiltrating the porous material laterally by surrounding the porous material with a thin impermeable membrane sealing its sides, letting the fluid infiltrate only at one end. Apart for slight

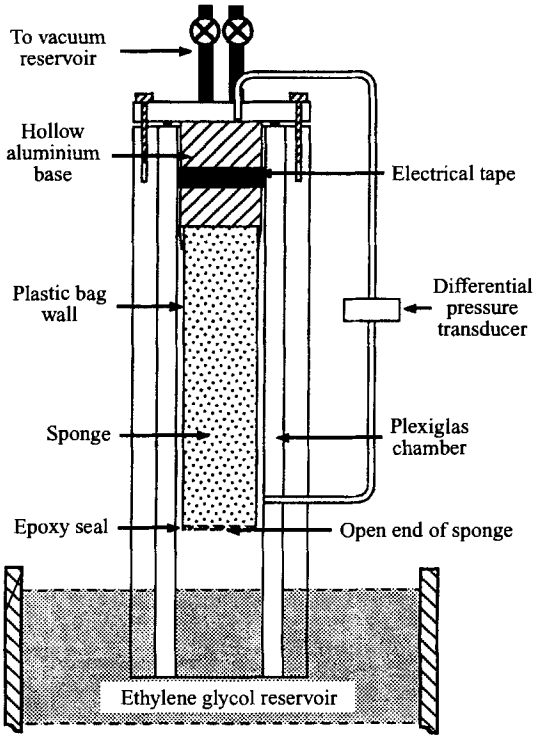

FIGURE 4. Schematic of the apparatus used to infiltrate the sponge with ethylene glycol.

loss of unidirectionality, there is no perturbation of fluid flow along the edge of the porous body, while at the same time there is no friction. Provided the rate of expansion of the porous solid during infiltration remains smaller than the infiltration front velocity, the only modification to the governing equations resulting from the lateral expansion is the replacement of (18) with (34), as explained in §2.3.

In addition to the relief this approach provides from friction or edge effects commonly found in unidirectional flow experiments, in this configuration the local strain within the porous material during infiltration can be directly measured with good precision from its local width distribution (since the lateral strain equals the longitudinal strain). Additionally, mechanical characterization and prestraining of the porous material is somewhat simplified in this configuration, as shown in §3.3.

The infiltration apparatus is shown schematically in figure 4. Its chamber was made of Plexiglas and had inside dimensions of 50.8 mm × 50.8 mm. The Plexiglas backing consisted of a hollow aluminium base, two outlets for the vacuum reservoir, a manual vent, and an inlet for the pressure transducer. The hollow aluminium base was machined to fit loosely inside the infiltration chamber and then sealed to the Plexiglas backing with silicone rubber and epoxy to produce a vacuum seal. A 2.54 cm thick aluminium honeycomb along with a stainless steel screen (24 Tyler mesh) were glued with epoxy within the aluminium base to act as supports for the sponge.

The sides of the sponge were surrounded by a transparent plastic bag 19 μm thick, which was hermetically sealed so as to allow the sponge to be somewhat loose inside the bag. The outer edges on one end of the sponge were sealed to the ends of the open bag by a thin 1 mm layer of epoxy to prevent the bag from moving during infiltration. The other end of the sponge was supported on the aluminium base. The surrounding

bag continued halfway over the outside surface of the aluminium base and was sealed to the sides of the base. This configuration allowed liquid infiltration to occur only through the front face of the sponge, opposite the aluminium base.

Constant vacuum at the sponge end near the aluminium base was achieved by connecting the back of the aluminium base to a large 160 litre vacuum reservoir via two 1.27 cm i.d. hoses. Vacuum could then be rapidly applied to the bottom of the sponge by opening two solenoid valves connected to the vacuum hoses. The open end of the infiltration chamber was submerged in a large vat of ethylene glycol containing coloured dye. The entrance of the infiltration chamber was suspended away from the bottom of the vat by a porous metal brace, built in such a way as to support the chamber during infiltration while allowing unimpeded liquid flow into the chamber mouth. A mercury thermometer was used to monitor the temperature of the fluid. A differential pressure transducer (Omega Engineering Inc., Stamford, CT) was used between the top of the sponge and the inside of the hollow aluminium base to allow the continuous measurement of the pressure drop across the sponge during infiltration.

A Panasonic AG-1830 digital video cassette recorder (VCR) was used to record and then replay the infiltration event one still field (1/60 s) at a time. The ability to monitor progression of the infiltration front was improved significantly by using digital enhancement of the image contrast. This produced a clearer visual distinction between the infiltrated and uninfiltrated portions of the sponge.

In an infiltration experiment, the moment when the infiltration front first contacted the sponge was defined as $t = 0$. The infiltration front position was then recorded with time. By knowing the position of the infiltration front and the sponge entrance, χ (defined in (10)) was calculated for each line drawn on the face of the infiltrated portion of the sponge. The width of the sponge at that point was used to measure the local θ of the sponge, and deduce the local liquid pressure at that point knowing the experimental curve of θ *vs.* hydrostatic pressure.

3.3. *Hydrostatic compression tests*

Two experiments were performed to characterize the foam before actual infiltration by the liquid. These were: (i) measurements of the foam volume-fraction porosity, θ, at different hydrostatic pressure, P, and (ii) tests of the viscoelastic behaviour of the sponge.

(i) θ *vs.* P. The foam was placed inside a sealed plastic bag from which the air was evacuated into a vacuum reservoir, and sponge dimensions were measured for various values of internal pressure. A thin 'buffer' sponge was used at the entrance of the vacuum reservoir port to shield the sponge used for infiltration from distortion caused by the vacuum port. Initial measurements were taken approximately 3 min after the sponge was totally evacuated, and the sponge was allowed to equilibrate for 40 s before measurements were taken after each increment in internal gas pressure, from full vacuum to atmospheric pressure. From the measured dimensions of the sponge, θ for a given hydrostatic pressure was then deduced, knowing the sponge weight. These tests were performed twice within a two-hour interval to verify reproducibility of the measurement.

(ii) *Viscoelastic behaviour tests.* Strain changes in the sponge held under a constant hydrostatic pressure for both short and long time periods were measured by evacuating the sponge enclosed in a plastic bag and by measuring the width of the sponge over a duration of 40 min, starting from the moment when the vacuum was first applied.

3.4. *Foam permeability measurements*

Although we neglect the progressive nature of infiltration by making the slug-flow approximation, permeability measurements were performed so as to duplicate the local liquid pressure and volume-fraction solid simultaneously present in the sponge during infiltration. Therefore, permeability was measured for variable foam volume fractions with average liquid pressures corresponding to one atmosphere minus the mechanical hydrostatic stress required to compress the preform to that volume fraction.

This was achieved by enclosing the foams in four aluminium boxes, corresponding to 25.2, 29.7, 37 and 52.2 kPa, having appropriate widths and lengths derived from the hydrostatic pressure experiments on the dry sponge before infiltration. Sponges of the appropriate size and orientation were then inserted in each box by first surrounding the sponge pieces with a plastic bag, evacuating the bag, and letting it expand after insertion in the aluminium box.

The permeability of sponges within these boxes was then measured with a falling head permeameter (Lambe & Whitman 1979) in which the average liquid pressure was maintained equal to the atmospheric pressure minus the stress corresponding to the dimensions of the sponge in the box. The pressure head driving flow of the liquid produced negligible compression of the prestrained sponge during the experiment.

Saturation was determined by closing the valve on the base of the sponge and then measuring the liquid drop after atmospheric pressure had been applied on top of the liquid, assuming that the sponge is completely saturated at atmospheric pressure. Knowing the liquid drop volume and the volume of the enclosed sponge, the liquid saturation could be calculated. The temperature of the liquid was measured immediately after the permeability experiment.

4. Experimental results

4.1. *Hydrostatic pressure vs.* θ

The results of the hydrostatic pressure test are shown in figure 5. The curves resemble qualitatively those of Beavers & Wilson (1975), Parker *et al.* (1987) and Lanir *et al.* (1990). There was no noticeable difference between data from two tests performed two hours apart from each other. For calculations, the average of both curves was fit with a seventh-order polynomial:

$$\sigma = A + B^*(1-\theta) + C^*(1-\theta)^2 + \ldots H^*(1-\theta)^7, \tag{43}$$

where $A = -2.329164 \times 10^7$ Pa; $B = 7.1349318 \times 10^8$ Pa; $C = -9.255285 \times 10^9$ Pa; $D = 6.597487 \times 10^{10}$ Pa; $E = -2.791823 \times 10^{11}$ Pa; $F = 7.0165383 \times 10^{11}$ Pa; $G = -9.702267 \times 10^{11}$ Pa and $H = 5.698018 \times 10^{11}$ Pa. The error in measuring θ was calculated to be about 5%.

4.2. *Viscoelastic behaviour of the sponge*

Curves of sponge solid fraction $(1-\theta)$ *vs.* time are shown in figure 6. As seen from figure 6(*a*), θ changes relatively little after the vacuum has been applied for more than 20 s, the change in θ being approximately 0.012 between 20 and 60 s. $(1-\theta)$ for longer relaxation times is shown in figure 6(*b*). The average θ of the sponge between 20 and 60 s is higher than its value at 40 min by only about 0.02; hence the sponge reaches a pseudo-steady state condition in 20 s, and continues to relax very slowly afterwards.

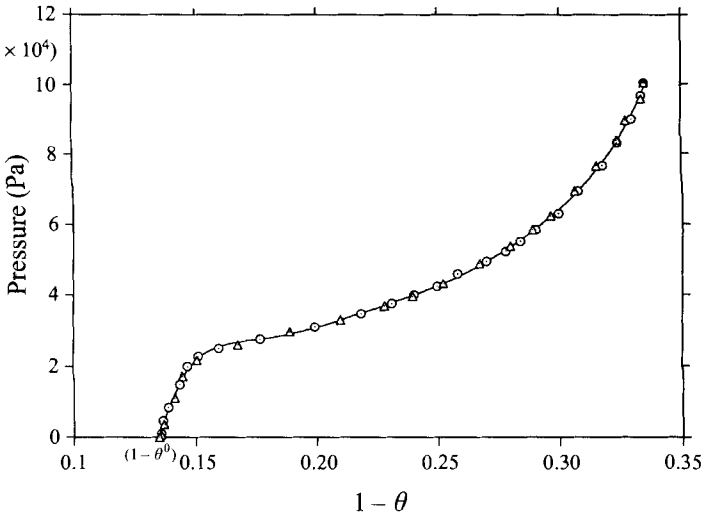

FIGURE 5. Plot of the results for two separate foam hydrostatic pressure tests, done approximately two hours apart on the same sponge used for the infiltration experiment.

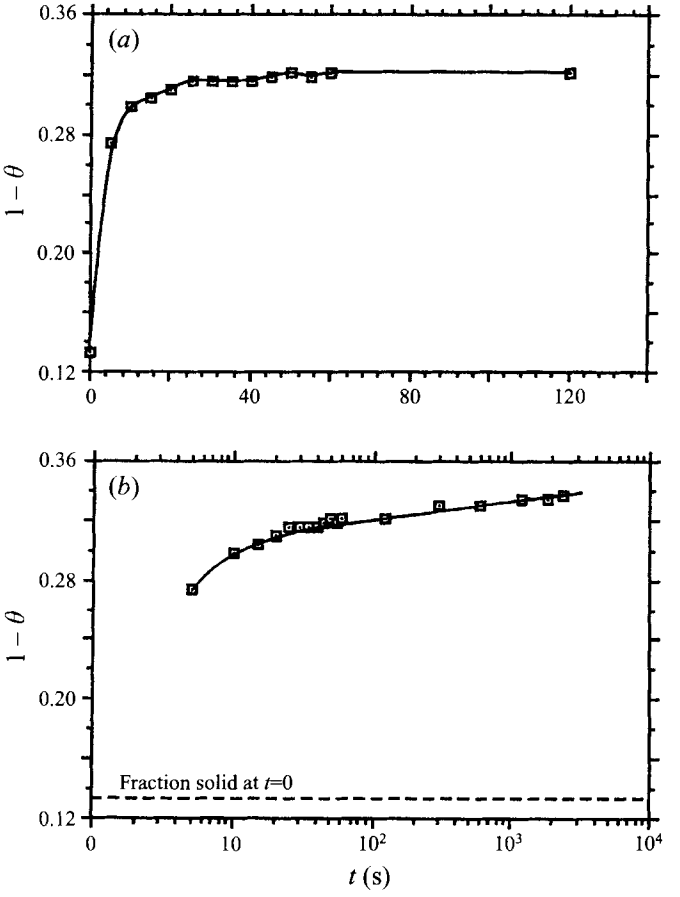

FIGURE 6. Plot of volume-fraction solid in the sponge under 0.1 MPa hydrostatic pressure (*a*) for short times (0 to 60 s) and (*b*) for longer times (1 s to 40 min).

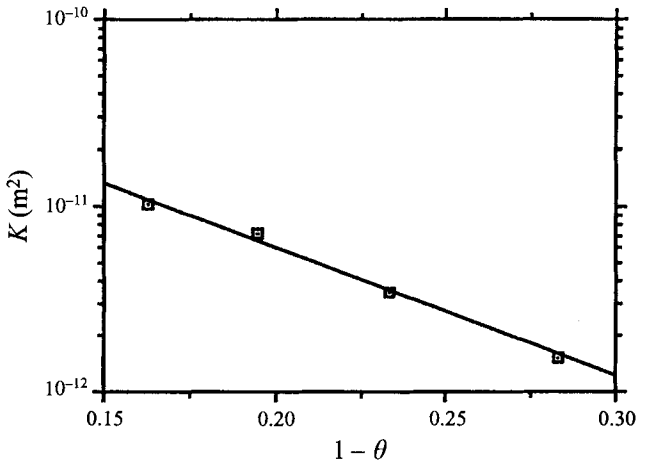

FIGURE 7. Experimental sponge permeability K as a function of volume fraction. The straight line corresponds to $K = 1.4729 \times 10^{-10}\ \text{m}^2 \times 10^{(-6.9654(1-\theta))}$.

Effective stress (MPa)	Liquid pressure (MPa)	V_s	K (m^2)	θ_v unsaturated void fraction
0.025	0.075	0.163	1.0×10^{-11}	0
0.03	0.07	0.195	7.1×10^{-12}	0.005
0.037	0.063	0.234	3.5×10^{-12}	0.013
0.052	0.048	0.283	1.5×10^{-12}	0.025

TABLE 1. Polyurethane foam permeability

4.3. *Sponge permeability*

Table 1 summarizes sponge permeability measurements. As shown in figure 7, the data points are fitted well by an exponential curve:

$$K = K_0 \times 10^{(-M(1-\theta))}, \tag{44}$$

where K_0 and M are 1.4729×10^{-10} m^2 and 6.9654, respectively. The error calculated for the permeability is approximately 10%.

In table 1, θ_v represents the fraction of unfilled void space at a total pressure of one atmosphere and liquid pressure P, assuming that there is complete saturation at $P = 1$ atmosphere. It was also observed that the ethylene glycol did not spontaneously wet the sponge, i.e. θ_v equals 1.0 for a liquid pressure $P = 0$. It is seen that the values of the unsaturated void fraction are finite, but very small.

4.4. *Experimental results for sponge infiltration*

The temperature of the ethylene glycol immediately before infiltration was 25.8 °C. The pressure drop registered between the infiltration front and the back of the sponge during the actual event was 99.5 kPa. Various times during the infiltration are reproduced from the video images in figures 8(*a*)–8(*d*). In these figures, the infiltration front is highlighted using the digital video recorder, as described above. Slight differences in response were found between the vertical and horizontal directions on the video monitor: the magnification factor differed slightly with direction, and the image

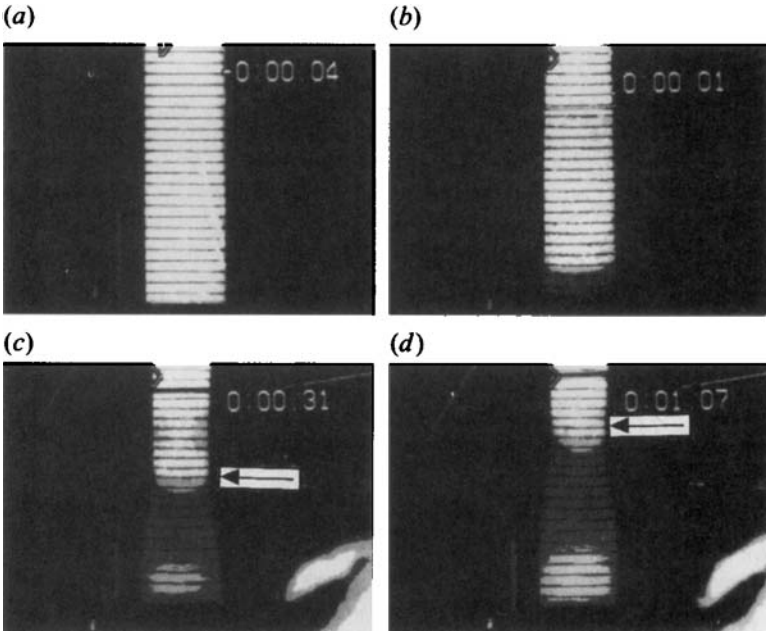

FIGURE 8. VCR images of sponge infiltration experiment at (*a*) $t < 0$ s, (*b*) $t = 1$ s, (*c*) $t = 31$ s, (*d*) $t = 67$ s. Light reflection effects caused variations in the shading of the infiltrated region, which varied from dark grey to light grey near the infiltration front and the porous-medium entrance. The infiltration front is therefore visible as the separation line between white uninfiltrated, and light grey infiltrated areas of the sponge, marked with an arrow on the figures.

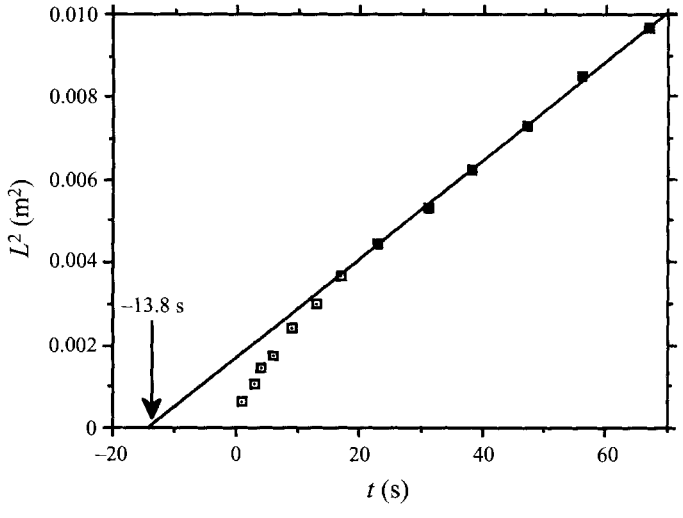

FIGURE 9. Total infiltrated length L^2 as a function of time.

enhancement program of the video recorder added 1.0 mm to the visible widths of the sponge, while leaving vertical features unaffected. These effects were taken into account in data collection.

The plot of L^2 *vs.* time in figure 9 shows that the curve becomes a straight line after approximately 17 s. The value of ψ^2-obtained from the slope of the line was

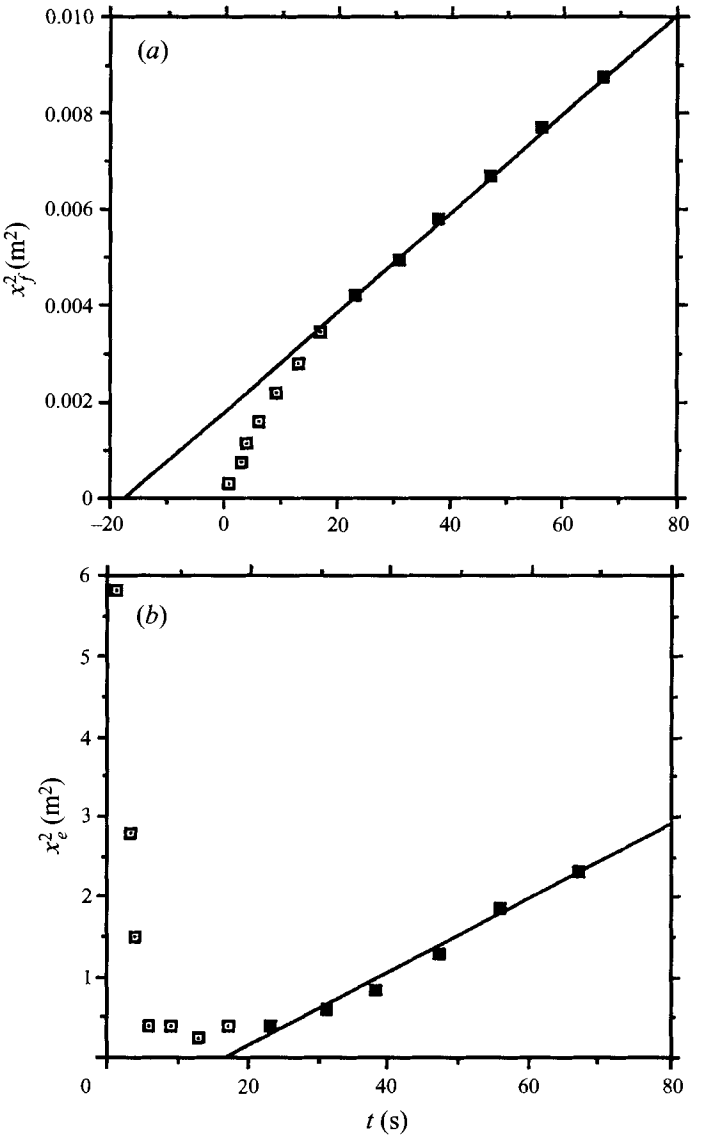

FIGURE 10. (*a*) Squared distance from $x = 0$ to the infiltration front as a function of time. (*b*) Squared distance from the sponge entrance to $x = 0$ as a function of time.

1.2×10^{-4} m^2 s^{-1} with an experimental error of 10%. Plots of x_f^2 and x_e^2 versus t are given in figures 10(*a*) and 10(*b*), respectively.

The measured volume fraction solid $(1-\theta)$ in the sponge *vs.* χ during infiltration is shown in figure 11. As the infiltration front moves through the sponge, the volume fraction profile within the infiltrated portion of the sponge should remain constant in this transformed axis. At earlier times, the curves tend to be shifted more to the left, i.e. to smaller values of θ. At longer times, greater than 17 s, the sponge profile tends to stabilize, although there still is a very small shift to the right as the sponge continues to relax.

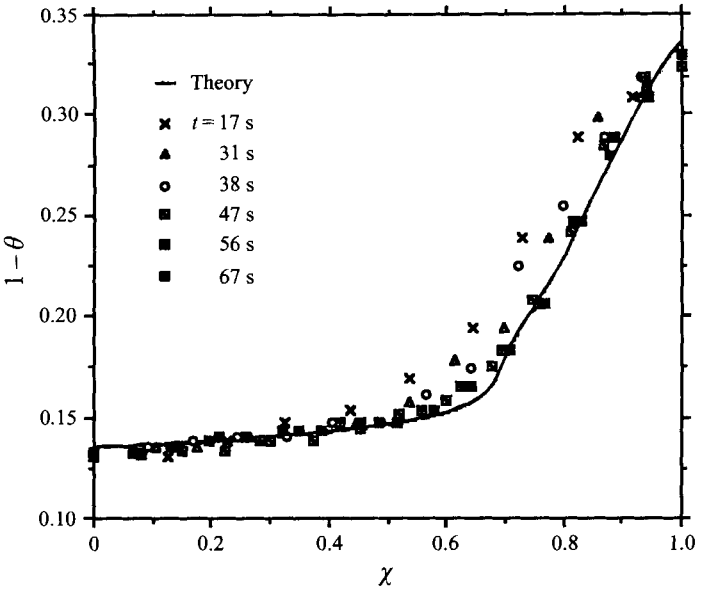

FIGURE 11. Experimental volume-fraction solid distribution along the infiltrated length of the sponge at various times, compared with theoretical predictions.

5. Discussion

5.1. *Assumptions of the model*

(i) *Darcy's law.* For Darcy's law to be valid, the Reynolds number Re, defined by

$$Re = d\rho v_l/\mu, \tag{45}$$

where d is the pore diameter of the porous medium, should be lower than a value of about 1. This corresponds to a maximum liquid velocity of 0.03 m s^{-1} (the viscosity and density of ethylene glycol being 15.7×10^{-3} Pa s and 1.109 g cm^{-3}, respectively). With $L^2 \approx 1.2 \times 10^{-4}$ t (figure 9), $\mathrm{d}L/\mathrm{d}t$ reaches 0.03 m s^{-1} after about 0.03 s, which is much smaller than the duration of the experiment. Hence, the time for the liquid velocity to fall everywhere below the limit set by (45) is trivial on the scale of the experiment, and flow is Darcian. The influence of gravity is negligible during the infiltration experiment: the maximum infiltration distance measured vertically was 9.8 cm, which corresponds to a pressure drop of 1.1 kPa, i.e. an error of 1 %, compared to the pressure drop across the sponge during the infiltration, which was 99.5 kPa.

(ii) *Wetting and permeability.* The first drainage curve of the dry uncompressed sponge was measured to determine the degree of saturation with applied pressure. There was no spontaneous infiltration, but when the applied pressure is 14.2 kPa, the liquid fills approximately 89 % of the pore space. Therefore, ΔP_γ at the infiltration front is positive, and significantly lower than 98 kPa. From (5), ΔP_γ should increase owing to compression of the sponge by a factor of only $(\theta^0/\theta^c) \approx 1.3$, when total atmospheric pressure is applied on the sponge, thus remaining significantly below 14.2 kPa. We have therefore assumed in our calculations that $\Delta P_\gamma = 0$.

As the applied pressure varies, the saturation changes little. Knowing that small deviations from full saturation exert only a small influence on relative permeability of a porous medium with a non-wetting fluid (Dullien 1979; Anderson 1987; Morel-Seytoux 1969), variations in the permeability K of the sponge with applied pressure are mostly due to variations in θ.

The equation found by Barry & Aldis (1990) for permeability of a polyurethane sponge from data of Parker *et al.* (1987) for unidirectional steady-state flow of liquid did not fit the permeability data as well as (44), and so was not used.

(iii) *Experimental error in θ and χ.* θ was measured using the width of the sponge; the largest error in θ was at the infiltration front, and is estimated at about 4%. The error in measuring χ, the fractional length along the infiltrated sponge, results mostly from slight curvature of the lines drawn on the sponge in the more distorted regions, located between $\chi = 0.65$ and 0.85. The largest error occurs when L, χ, and infiltration times are relatively small. At $t = 23$ s and $\chi = 0.68$, a maximum error of about 4% was calculated.

(iv) *Effects of air evacuation and viscoelasticity.* As infiltration of the sponge only lasted approximately one minute, some error is introduced owing to incomplete relaxation of the sponge during infiltration compared to data in the curve of figure 6. This was estimated to introduce a total error in θ of 0.09.

(v) *Effect of evaporation at the infiltration front.* Boiling of the ethylene glycol infiltrant could have occurred at the infiltration front owing to the vacuum, though it was not discernable at the liquid–vacuum interface during infiltration. The resulting temperature drop at the infiltration front was estimated to be approximately -0.01 K, which does not influence the infiltration kinetics noticeably (Sommer 1992).

(vi) *Influence of the fluid on mechanical properties of the sponge.* Beavers *et al.* (1981*b*) noticed that water-submerged sponges would strain to a further degree under a given applied stress than when in the dry state. This was attributed to liquid lubrication effects that may have occurred within the internal structure of the wet sponge during compression. Since all mechanical testing on the sponge was done in the dry state (to prevent complications in the results induced by flow of the liquid), some added experimental error in the mechanical relaxation properties of the sponge may have resulted from this effect.

5.2. *Comparison of theory with experiment*

Experimental data show that after about 17 s, plots of L^2, x_f^2, and x_e^2 versus t, figures 9 and 10, all become linear. Since mechanical tests show that time dependence in the mechanical behaviour of the sponge becomes negligible after at most 20 s, we conclude that the experimental data confirm the analysis. This time dependence of infiltration parameters has been observed in previous work on flow of water into swelling soils (Smiles & Rosenthal 1968; Smiles & Colombera 1975).

ψ^2 was measured to be 1.2×10^{-4} m^2 s^{-1} while theory predicts 9.1×10^{-5} m^2 s^{-1}. At the infiltration front, l was measured to be 0.96 while the theoretical value obtained was 0.80. Experimental error in the measured value of ψ^2 is 10%. The uncertainty in the predicted value of ψ^2 is roughly proportional to the uncertainty in the permeability, K. The uncertainty in K that arises from experimental error in the correlation between K and θ is on the order of $\Delta K/K \approx 12\%$. The experimental error in the measurement of θ, $\Delta\theta/\theta \approx 4\%$ introduces additional uncertainty in the predicted permeability, on the order of 60%. The predicted rate of infiltration, measured by ψ^2, is therefore well within experimental error of the measured value.

Figure 11 shows the volume fraction along the infiltrated sample at different times, and compares these data with theory. For $t > 20$ s, the curve is invariant in time, in agreement with theory and with previous work on flow of water into swelling soils (Smiles & Rosenthal 1968; Smiles & Colombera 1975). For $t < 20$ s, the curve is shifted somewhat to the left of the pseudo-steady-state value, as expected for incomplete relaxation of the sponge due to its viscoelastic behaviour. Comparison between

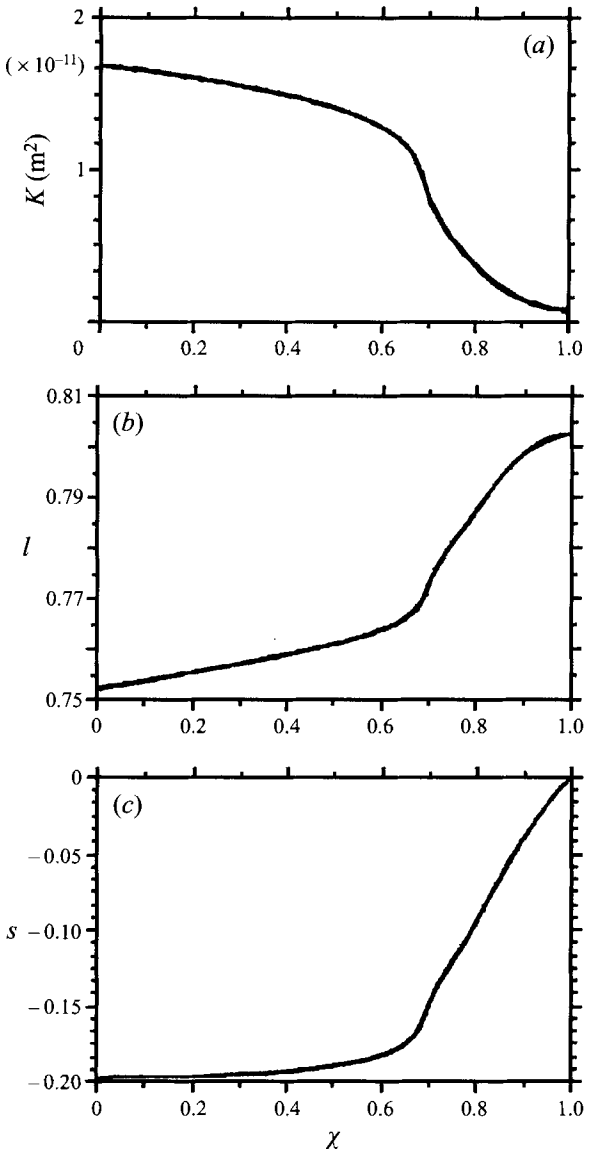

FIGURE 12. Theoretical predictions along infiltrated length for the experiment: (*a*) K, (*b*) l, and (*c*) s.

predicted and measured pseudo-steady-state curves of $(1-\theta)$ versus χ is very satisfactory. In particular, agreement of θ at the infiltration front with theory legitimizes the assumption made earlier that $\Delta P_\gamma \approx 0$.

The predicted curve of local permeability, K, as a function of χ during infiltration is shown in figure 12(*a*). K tends to drop off precipitously at lower θ, near the infiltration front. This region therefore constitutes a 'bottleneck' to infiltration, and dominates the kinetics of the process. Predicted curves of l and s as a function of χ are shown in figures 12(*b*) and 12(*c*). It is seen that l and s, as well as θ (figure 11), vary rapidly behind the infiltration front, and reach relatively steady values for $\chi \leqslant 0.65$.

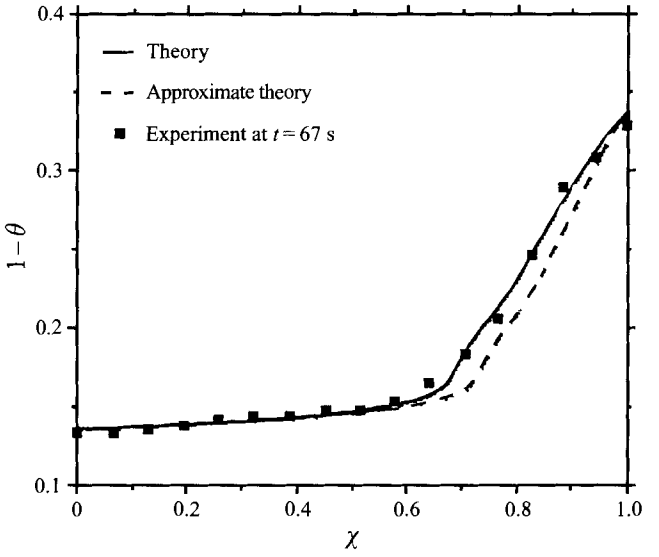

FIGURE 13. Comparison of volume fraction solid *vs.* χ for the theory of §§ 2.2 and 2.3, the approximate theory of §2.5, and experimental data at 67 s.

5.3. *Comparison of approximate theory with experiment*

We now test the additional approximation of neglecting v_s compared to v_l, introduced in §2.5. By insertion of (43) and (44) into (42) and numerical integration (using Mathematica™, software trademark of Wolfram Research Inc., Champaign, Ill.), Ψ^2 is now predicted to equal 1.04×10^{-4} m^{-2} s^{-1}. This corresponds to an increase in Ψ, and hence in the predicted rate of infiltration, of 7% compared to the more precise analysis. Keeping in mind the very high rate of variation of permeability K with θ, the error introduced is thus small. The predicted distribution of fraction solid $(1-\theta)$ versus fractional infiltrated length χ, figure 13, shows less good agreement with experiment than the more precise analysis, but provides nonetheless a very acceptable prediction considering the much greater ease of calculation.

The error introduced in making the simplifying assumption of §2.5, namely neglecting u_s compared to u_l or equivalently s compared to l and, hence, 1, can be tested for consistency by estimation of $s(0)$ via a simple macroscopic mass balance:

$$s(0) \approx \int_0^1 \frac{(1-\theta)\,\mathrm{d}\chi}{1-\theta^c} - 1. \tag{46}$$

Since $-s(\chi) \leqslant -s(0)$ everywhere, then, the relative error introduced by the approximation of §2.5 in the predicted rate of infiltration, Ψ, should be at most on the order of $s(0)$ estimated above. Comparing $s(0)$ from (46) to 1 therefore provides a simple test of the error introduced in using the approximate method of §2.5.

6. Conclusions

Flow of a pressurized liquid into a deformable porous medium can be analysed using the slug-flow assumption when the applied pressure exceeds significantly the capillary pressure for full saturation of the porous medium with the liquid. This assumption reduces significantly the number of system parameters required to predict flow rates in the porous medium, and thus simplifies considerably the problem. We apply this

assumption to treat unidirectional horizontal infiltration driven by constant pressure using the Boltzmann transformation.

Experiments performed on a polyurethane sponge in near-unidirectional infiltration with hydrostatic strain compare well with theoretical predictions after an initial transient resulting largely from viscoelasticity in the sponge behaviour. Predicted infiltration rates and strain distributions within the porous medium are in quantitative agreement with the analysis, and thus confirm the validity of its simplifying assumptions.

Neglecting the solid-phase velocity compared with that of the liquid reduces the mathematical solution of the problem to a single numerical integration of measurable materials parameters. This simplification provides a reasonable estimate of infiltration kinetics and porous-medium strain distribution because solid-phase velocities are lowest near the infiltration front, where permeability is lowest, and θ variations highest. This approximate model agrees relatively well with the experimental data.

The principal conclusion from this work is that analysis of infiltration with significant applied loads and porous-medium deformation can be conducted using the slug-flow approximation. This approximation reduces very significantly the number of relevant materials parameters and, hence, the number of necessary measurements of porous medium properties, since partial saturation and its influence on permeability and porous-medium rheology need not be considered.

We gratefully acknowledge sponsorship of this work by ALCOA under the supervision of Dr Warren Hunt.

REFERENCES

ANDERSON, W. G. 1987 Wettability literature survey – Part 5: The effects of wettability on relative permeability. *J. Petrol. Technol.* **39**, 1453–1468.

ANGULO, R., GAUDET, J. P., THONY, J. L. & VAUCLIN, M. 1990*a* Conductivité hydraulique d'un milieu poreux partiellement saturé, déformable. I. Principes de détermination. *C. R. Acadé. Sci. Paris* **310** (II), 161–164.

ANGULO, R., GAUDET, J. P., THONY, J. L. & VAUCLIN, M. 1990*b* Conductivité hydraulique d'un milieu poreux partiellement saturé, déformable. II. Résultats expérimentaux. *C. R. Acadé. Sci. Paris* **310** (II), 341–345.

BARRY, S. I & ALDIS, G. K. 1990 Comparison of models for flow induced deformation of soft biological tissue. *J. Biomech.* **23**, 647–654.

BEAR, J. 1972 *Dynamics of Fluids in Porous Media*, pp. 206, 303, and 519. Elsevier.

BEAR, J. & BACHMAT, Y. 1990 *Introduction to Modeling of Transport Phenomena in Porous Media*, p. 305. Kluwer.

BEAVERS, G. S., HAJJI, A. & SPARROW, E. M. 1981*a* Fluid flow through a class of highly deformable porous media, Part I: Experiments with air. *Trans. ASME* I: *J. Fluids Engng* **103**, 432–439.

BEAVERS, G. S. & WILSON, T. A. 1975 *Flow through a deformable porous material. Trans. ASME* E: *J. Appl. Mech.* **42**, 598–602.

BEAVERS, G. S., WITTENBERG, K. & SPARROW, E. M. 1981*b* Fluid flow through a class of highly deformable porous media, Part II: Experiments with water. *Trans. ASME* I: *J. Fluids Engng* **103**, 440–444.

BIOT, M. A. 1955 Theory of elasticity and consolidation for a porous anisotropic solid. *J. Appl. Phys.* **26**, 182–185.

DAVE, R. 1990 A unified approach to modeling resin flow during composite processing. *J. Composite Mater.* **24**, 23–41.

DULLIEN, F. A. L. 1979 *Porous Media, Fluid Transport and Pore Structure*, pp. 257–283. Academic.

GREEN, W. H. & AMPT, G. A. 1911 Studies on soil physics. Part I. – The flow of air and water through soils. *J. Agric. Sci* **4** (May), 1–24.

GUTOWSKI, T. G., MORIGAKI, T. & CAI, Z. 1987 The consolidation of laminate composites. *J. Composite Mater.* **21**, 172–188.

LAL, R., BRIDGE, B. J. & COLLIS-GEORGE, N. 1970 The effect of column diameter on the infiltration behaviour of a swelling soil. *Austral. J. Soil Res.* **8**, 185–193.

LAMBE, T. W. & WHITMAN, R. V. 1979 *Soil Mechanics*, pp. 281–292. John Wiley and Sons.

LANIR, Y., SAUOB, S. & MARETSKY, P. 1990 Nonlinear finite deformation response of open cell polyurethane sponge to fluid filtration. *Trans. ASME* E: *J. Appl. Mech.* **57**, 449–454.

MASUR, L. J., MORTENSEN, A., CORNIE, J. A. & FLEMINGS, M. C. 1989 Infiltration of fibrous preforms by a pure metal: Part II. Experiment. *Metall. Trans.* **20A**, 2549–2557.

MOREL-SEYTOUX, H. J. 1969 Introduction to flow of immiscible liquids in porous media. In *Flow through Porous Media* (ed. R. J. M. D. Wiest), pp. 455–516.

MORTENSEN, A. 1990 Corrigenda and comments on the infiltration of fiber preforms. *Metall. Trans.* **21A**, 2287.

MORTENSEN, A., MASUR, L. J., CORNIE, J. A. & FLEMINGS, M. C. 1989 Infiltration of fibrous preforms by a pure metal: Part I. Theory. *Metall. Trans.* **20A**, 2535–2547.

MORTENSEN, A. & WONG, T. 1990 Infiltration of fibrous preforms by a pure metal: Part III. Capillary phenomena. *Metall. Trans.* **21A**, 2257–2263.

NUR, A. & BYERLEE, J. D. 1971 An exact effective stress law for elastic deformation of rock with fluids. *J. Geophys. Res.* **76**, 6414–6419.

PARKER, K. H. & MEHTA, R. V. & CARO, C. G. 1987 Steady flow in porous, elastically deformable materials. *Trans. ASME* E: *J. Appl. Mech.* **54**, 794–800.

PHILIP, J. R. 1968 Kinetics of sorption and volume change in clay-colloid pastes. *Austral. J. Soil Res.* **6**, 249–267.

PHILIP, J. R. 1969*a* Hydrostatics and hydrodynamics in swelling soils. *Water Resources Res.* **5**, 1070–1077.

PHILIP, J. R. 1969*b* Theory of infiltration. In *Advances in Hydroscience*, *5* (ed. V. T. Chow), pp. 215–297. Academic.

PHILIP, J. R. & SMILES, D. E. 1969 Kinetics of sorption and volume change in three-component systems. *Austral. J. Soil Res.* **7**, 1–19.

PRESS, W. H., FLANNERY, B. P., TEUKOLSKY, S. A. & VETTERLING, W. T. 1989 *Numerical Recipes: The Art of Scientific Computing* (*Fortran version*), pp. 271, 551, 583. Cambridge University Press.

SCHEIDEGGER, A. E. 1974 *The Physics of Flow through Porous Media*, p. 84. Toronto Press.

SMILES, D. E. & COLOMBERA, P. M. 1975 Early stages of infiltration into a swelling soil. In *Proc. Seminar on Heat and Mass Transfer in the Environment of Vegetation* (ed. D. A. deVries & N. H. Afgan), pp. 77–85. Halsted.

SMILES, D. E. & ROSENTHAL, M. J. 1968 The movement of water in swelling materials. *Austral. J. Soil Res.* **6**, 237–248.

SOMMER, J. L. 1992 Infiltration of deformable porous media. PhD thesis, Department of Materials Science and Engineering, Massachusetts Institute of Technology.

YAMAUCHI, T. & NISHIDA, Y. 1995 Infiltration kinetics of fibrous preforms by aluminum with solidification. *Acta Metall. Mater.* **43**, 1313–1321.

YANG, Y. W., ZOGRAFI, G. & MILLER, E. E. 1988 Capillary flow phenomena and wettability in porous media. II – Dynamic flow studies. *J. Colloid Interface Sci.* **122**, 35–46.